© 2014. Published by The Company of Biologists Ltd | The Journal of Experimental Biology (2014) 217, 2181-2192 doi:10.1242/jeb.083907

RESEARCH ARTICLE

The length–force behavior and operating length range of squid muscle vary as a function of position in the mantle wall

Joseph T. Thompson[1,*], Ryan M. Shelton[2] and William M. Kier[2]

ABSTRACT

Hollow cylindrical muscular organs are widespread in animals and are effective in providing support for locomotion and movement, yet are subject to significant non-uniformities in circumferential muscle strain. During contraction of the mantle of squid, the circular muscle fibers along the inner (lumen) surface of the mantle experience circumferential strains 1.3 to 1.6 times greater than fibers along the outer surface of the mantle. This transmural gradient of strain may require the circular muscle fibers near the inner and outer surfaces of the mantle to operate in different regions of the length–tension curve during a given mantle contraction cycle. We tested the hypothesis that circular muscle contractile properties vary transmurally in the mantle of the Atlantic longfin squid, *Doryteuthis pealeii*. We found that both the length–twitch force and length–tetanic force relationships of the obliquely striated, central mitochondria-poor (CMP) circular muscle fibers varied with radial position in the mantle wall. CMP circular fibers near the inner surface of the mantle produced higher force relative to maximum isometric tetanic force, P_0, at all points along the ascending limb of the length–tension curve than CMP circular fibers near the outer surface of the mantle. The mean ± s.d. maximum isometric tetanic stresses at L_0 (the preparation length that produced the maximum isometric tetanic force) of 212±105 and 290±166 kN m^{-2} for the fibers from the outer and inner surfaces of the mantle, respectively, did not differ significantly (P=0.29). The mean twitch:tetanus ratios for the outer and inner preparations, 0.60±0.085 and 0.58±0.10, respectively, did not differ significantly (P=0.67). The circular fibers did not exhibit length-dependent changes in contraction kinetics when given a twitch stimulus. As the stimulation frequency increased, L_0 was approximately 1.06 times longer than L_{TW}, the mean preparation length that yielded maximum isometric twitch force. Sonomicrometry experiments revealed that the CMP circular muscle fibers operated *in vivo* primarily along the ascending limb of the length–tension curve. The CMP fibers functioned routinely over muscle lengths at which force output ranged from only 85% to 40% of P_0, and during escape jets from 100% to 30% of P_0. Our work shows that the functional diversity of obliquely striated muscles is much greater than previously recognized.

KEY WORDS: Cephalopod, Obliquely striated muscle, Operating length range, Length–force relationship, Transmural gradient of strain

INTRODUCTION

Hollow, cylindrical muscular organs and bodies are common in animals, especially soft-bodied invertebrates. Such body plans are effective in providing mechanical support for many forms of locomotion and movement (e.g. Clark, 1964; Wainwright, 1988), but recent work showed that they experience significant non-uniformity in circumferential strain across the thickness of the muscular body wall (Thompson et al., 2008; Thompson et al., 2010a). This phenomenon can be illustrated as follows. Imagine a cross-section of the cylindrical body wall. As long as (1) the body wall remains essentially constant in volume during shortening of the circumferential (i.e. circular) musculature (a reasonable assumption given the high bulk modulus of animal tissue), (2) the length does not change significantly, and (3) the circular muscle fibers remain oriented in the plane of section (i.e. their long axes remain perpendicular to the long axis of the body wall), the body wall must increase in thickness as the circular muscles shorten. The circular fibers near the inner lumen surface thus shorten proportionately more than the circular fibers near the outer surface for a given decrease in the diameter of the body.

Thompson et al. (Thompson et al., 2010a) investigated this phenomenon in the mantle, a cylindrical muscular organ that meets the three criteria specified above, of Atlantic longfin squid, *Doryteuthis pealeii*, and oval squid, *Sepioteuthis lessoniana*. They found that circular muscle fibers along the inner surface of the mantle experience circumferential strains 1.3 to 1.6 times greater than fibers along the outer surface of the mantle during the same contraction. This transmural gradient of strain implies that muscle fibers from the inner surface may operate on a different region of the length–tension curve than those on the outer surface at any point in the contraction cycle. Thus, fibers from a given region of the mantle wall may produce different instantaneous forces than those in other regions. Such transmural differences in force output by the circular fibers could reduce the mechanical efficiency of the mantle during contraction (Shadwick and Syme, 2008; van Leeuwen et al., 2008).

Because the circular fibers from near the inner surface of the mantle have significantly greater excursion ranges *in vivo* than circular fibers from near the outer surface of the mantle, we predict that fibers from near the inner surface will spend a smaller fraction of the contraction cycle in the region of maximum force of the length–tension curve. Different length–force relationships of the circular fibers near the outer versus the inner surfaces of the mantle might reduce the impact of such transmural differences in operating length range and potentially allow all of the circular fibers to generate similar instantaneous forces during mantle contraction. We hypothesize, therefore, that the circular muscle fibers near the inner surface produce higher forces, relative to the peak isometric force (P_0), on the ascending and descending limbs of the length–tension curve; i.e. the length–tension curve for the circular fibers from near the inner surface will have ascending and descending limbs with lower slopes. Our hypothesis assumes that all of the circular muscle fibers in the mantle operate on roughly similar regions of the length–tension curve during the mantle contraction cycle (i.e. there

[1]Department of Biology, Franklin & Marshall College, PO Box 3003, Lancaster, PA 17604-3003, USA. [2]Department of Biology, CB# 3280, University of North Carolina, Chapel Hill, NC 27599-3280, USA.

*Author for correspondence (joseph.thompson@fandm.edu)

Received 5 December 2013; Accepted 17 March 2014

The Journal of Experimental Biology (2014) doi:10.1242/jeb.083907

List of symbols and abbreviations

CMP	central mitochondria-poor
DML	dorsal mantle length
L_0	muscle preparation length that generated the maximum isometric tetanic force
L_{Slab}	distance between the pinholes on the tissue slabs glued to the vibratome stage
L_{TW}	muscle preparation length that generated the maximum isometric twitch force
P_0	peak isometric tetanic force
P_{TW}	peak isometric twitch force
SMR	superficial mitochondria-rich

is no transmural staggering of resting sarcomere lengths). Testing the hypothesis, therefore, also requires investigation of the *in vivo* operating length ranges of the circular muscles.

We tested the hypothesis in the mantle of the Atlantic longfin squid, *Doryteuthis pealeii* (Lesueur 1821). We first used sonomicrometry to measure muscle fiber length changes in the central mitochondria-poor (CMP) (Preuss et al., 1997) circular fibers near the outer and inner surfaces of the mantle during a range of locomotory behaviors. We then investigated the length–force relationship of bundles of CMP circular muscle fibers near the inner and outer surfaces of the mantle, and also examined potential transmural differences in other contractile properties, including length dependence of activation, the effect of stimulus frequency on the length–force relationship, twitch:tetanus ratio and maximum isometric stress. Finally, we developed a method to superimpose the two sets of data in order to identify where along the length–tension curve the muscle fibers operate *in vivo*.

RESULTS

Muscle mechanics

We obtained thorough sampling of the ascending limb of the length–twitch force relationship for CMP circular muscle preparations obtained from near the inner and outer surfaces of the mantle (Fig. 1A). We were unable, however, to sample the descending limb extensively at lengths beyond the force maximum region because preliminary studies revealed that preparations exhibited signs of damage, including an altered force–time trace (i.e. an approximate doubling of $T_{50\%}$, the half relaxation time) and an inability to produce peak isometric twitch force (P_{TW}) when returned to L_{TW} (the preparation length that produced P_{TW}). Data from damaged preparations were excluded from the results we present here. We also were unable to explore the ascending limb at lengths $<0.60L/L_{TW}$. The preparations resisted compression and buckled when we attempted to adjust them below this length when relaxed, yet appeared to contract when stimulated, suggesting that the circular fibers might be able to shorten even more *in vivo*.

The length–twitch force relationships of the two preparation types differed. On the ascending limb of the length–tension curve, the preparations from near the inner surface of the mantle generated higher force relative to P_{TW} than the preparations from near the outer surface at a given preparation length (Fig. 1A). At preparation lengths $\leq 0.95L_{TW}$, the ascending limbs were sufficiently linear to allow comparison of the slopes and *y*-intercepts of the two data sets. The circular muscle preparations from the inner surface of the mantle exhibited a significantly lower slope of the ascending limb (independent-samples *t*-test: t=3.84, d.f.=17, P=0.001) and higher *y*-intercept (t=–4.63, d.f.=17, P<0.001) than preparations from near the outer surface of the mantle (Fig. 1A). At a given length on the descending limb, the preparations from near the inner surface of the mantle also produced higher twitch force than the outer preparations. We were unable to explore the descending limb beyond $1.1L_{TW}$, however, and thus at this point our conclusions about the relative forces on the descending limb are tentative.

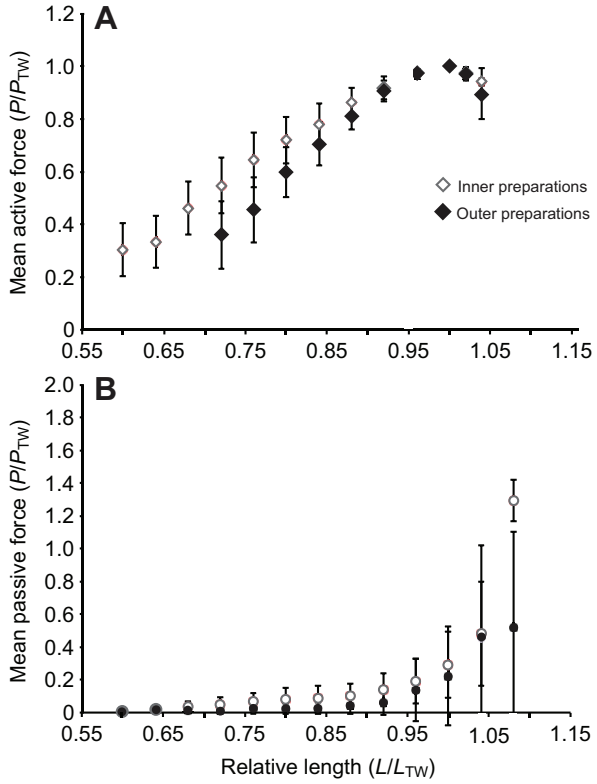

Fig. 1. Length–force relationship using twitch stimulation (2 ms pulse width) for the central mitochondria-poor (CMP) circular muscle fiber preparations from near the outer (black symbols) and inner (white symbols) surfaces of the mantle of *Doryteuthis pealeii*. Data were normalized by the preparation length (L_{TW}) that produced the highest isometric twitch force (P_{TW}). (A) Active force. Linear regressions were fit to the length–force data for each squid for the data at lengths $\leq 0.95L_{TW}$. The slopes of the ascending limbs differed significantly between the inner and outer preparations (independent-samples *t*-tests: t=3.84, P=0.001), as did the *y*-intercepts (t=–4.63, P<0.001). (B) Passive force. At each relative length listed, there was no significant difference in passive force between the two preparation types (independent-samples *t*-test; P>0.2 for all comparisons). For both A and B, the sample size was 10 squid (Group 1, see Materials and methods) for each type of preparation.

At each preparation length, the passive force (Fig. 1B), normalized to P_{TW}, did not differ significantly between preparations from the outer or inner surfaces of the mantle (independent-samples *t*-tests: P>0.2 for all comparisons).

The length–tetanic force relationship of the two preparation types also differed on the ascending limb, with preparations from near the inner surface producing higher force relative to P_0 (the maximum isometric tetanic force) at a given length than preparations from near the outer surface (Fig. 2). The preparations from the inner surface exhibited a significantly lower slope of the ascending limb ($\leq 0.95L_0$, t=2.91, d.f.=9, P=0.017) and higher *y*-intercept (t=–2.40, d.f.=9, P=0.04) than preparations from near the outer surface.

When stimulated tetanically, the mean (±s.d.) maximum isometric stresses (P_0) at L_0 (the preparation length that yielded P_0) were 212±105 kN m^{-2} (n=7) and 290±166 kN m^{-2} (n=8) for the preparations from the outer and inner surfaces of the mantle, respectively. The means did not differ significantly (t=–1.1, d.f.=13, P=0.29).

The Journal of Experimental Biology (2014) doi:10.1242/jeb.083907

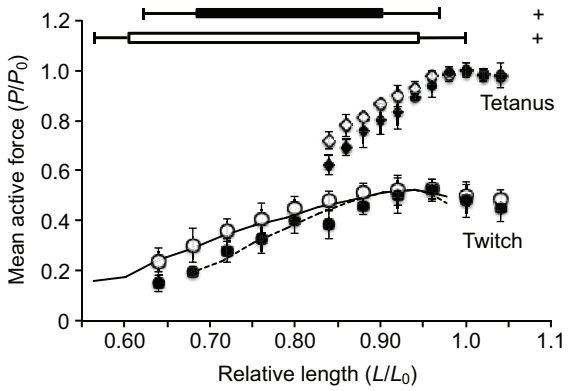

Fig. 2. Length–force relationship and *in vivo* operating length ranges of the circular muscle fibers from near the outer (filled symbols) and inner (open symbols) surfaces of the mantle. Length–force relationships for muscle preparations from the squid in Group 3 (see Materials and methods) for twitch (2 ms pulse width) and tetanic (2 ms pulses, 80 Hz, 100 ms duration) stimulations are shown. Solid (inner preparations) and dashed (outer preparations) lines represent the means of length–twitch force data from the squid in Group 1 (see Fig. 1A and Materials and methods). Group 1 data from Fig. 1A were aligned to the Group 3 length–twitch force data (indicated by the open and filled circles). Linear regressions were fit to the length–tetanic force data for each squid for the data at lengths ≤0.95L_0, where L_0 is the muscle preparation length that generated the maximum isometric tetanic force. The slopes of the ascending limbs differed significantly between the inner and outer preparations (independent-samples *t*-test: t=2.91, P=0.017), as did the *y*-intercepts (t=–2.40, P=0.04). The boxes (black, outer preparations; white, inner preparations) above the length–tension curves show the *in vivo* operating length ranges of the circular fibers from the squid in Group 1, and are in register with the length–twitch force data from these specimens (shown in Fig. 1A) and the Group 3 length–twitch force data. The right edge of each box shows the mean muscle length (relative to L_{TW}) in the fully expanded mantle just prior to the start of mantle contraction, while the left edge shows the mean muscle length at the end of mantle contraction. The whiskers encompass 75% of the data that fell above the mean (right for mantle expansion) or below it (left for mantle contraction). The + symbols represent the largest hyperinflations from each group. Box plot sample size: 111 escape jets from each group. The box plots include data from the two squid that operated in a primarily hyperinflated state (see Results).

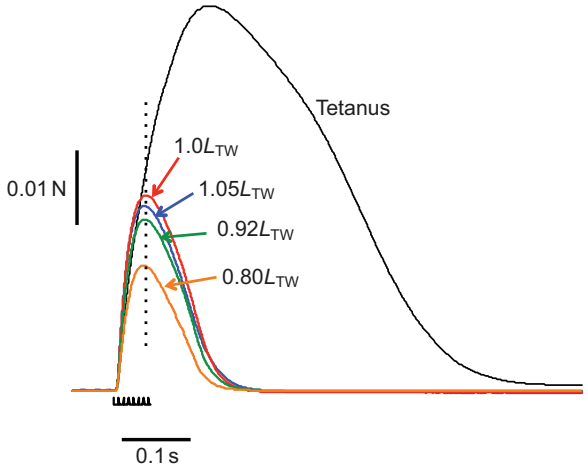

Fig. 3. Force–time traces for the mantle circular fibers. Four twitch force–time traces from the same preparation are superimposed to illustrate the absence of length-dependent changes in contraction kinetics in the mantle CMP circular muscle fibers. The vertical dotted line is centered on the peak of the twitch force trace at 1.0L_{TW} (the preparation length that produced the highest isometric twitch force). The force–time trace for tetanic stimulation (2 ms pulses, 80 Hz, 100 ms duration) for the same preparation is also illustrated. The timing of the tetanic stimuli is indicated by the tick marks below the curves. The twitch stimulus (2 ms pulse width) is indicated by the first tick mark.

The mean (±s.d.) twitch:tetanus ratios for the outer and inner preparations were 0.60±0.085 (n=10) and 0.58±0.10 (n=11), respectively. The means of the two preparation types did not differ significantly (t=–0.43, d.f.=19, P=0.67).

All of the muscle preparations exhibited two characteristics that differ from the cross-striated muscles of vertebrates and arthropods. First, the CMP circular muscles did not exhibit substantial length-dependent changes in contraction kinetics (i.e. length-dependent activation) when stimulated with a twitch stimulus. Both T_{max} (time from the onset of stimulation to the maximum force of the twitch) and $T_{50\%}$ increased slightly as preparation length increased (Fig. 3). The T_{max} increased from the shortest to the longest preparation lengths by (mean ± s.d.) 0.0057±0.0046 s (n=10) and 0.0069±0.0054 s (n=10) for the outer and inner preparations, respectively. The difference was not significant (t=0.688, d.f.=17, P=0.497). The $T_{50\%}$ increased from the shortest to the longest preparation lengths by 0.019±0.014 and 0.025±0.013 s for the outer and inner preparations, respectively (Fig. 3). The difference was not significant (t=1.32, d.f.=28, P=0.196). In addition, the slopes of the regressions of preparation length versus T_{max} and preparation length versus $T_{50\%}$ did not differ significantly between muscle preparations from the outer and inner surfaces of the mantle (T_{max}: t=–0.594, d.f.=17, P=0.563; $T_{50\%}$: t=–1.781, d.f.=17, P=0.106). Furthermore, the *y*-intercepts of the regressions did not differ significantly (T_{max}: t=–2.1, d.f.=17, P=0.08; $T_{50\%}$: t=–2.0, d.f.=17, P=0.085).

Second, L_0 was longer than L_{TW} for all preparations (Fig. 4A). For the outer (n=7) and inner (n=7) preparations, L_0 was 1.05±0.035 (mean ± s.d.) and 1.06±0.061 times longer, respectively, than L_{TW} (Fig. 4). We calculated the ratio of L_{TW} to L_0 for each preparation and found no significant difference between the means for the outer and inner preparations (t=–0.43, d.f.=13, P=0.68).

Mantle kinematics and *in vivo* muscle operating length range

The squid exhibited a diverse repertoire of jetting behaviors, ranging along a continuum from low-amplitude and low-frequency ventilatory jets to relatively stereotyped rapid, large-amplitude escape jets, with more variable jets used during slow swimming (i.e. ≤1 mantle length s^{-1}) in between (Fig. 5; see supplementary material Movies 1 and 2 for videos that illustrate swimming behavior). Two squid operated in a more-or-less hyperinflated state [i.e. contraction of the radial muscle fibers expands the mantle radially beyond the resting position, thus filling the mantle cavity with more water (see Gosline et al., 1983)] for most of the swimming trials whereas other individuals hyperinflated only during escape jets and isolated jets used during slow swimming.

All of the CMP circular muscle fibers operated almost exclusively on the ascending limbs of the length–twitch force and length–tetanic force relationships for all jets (Fig. 2; see Table 1 for the mean muscle operating length ranges). For escape jets, there was no significant transmural difference in muscle length at the start of mantle contraction (t=0.62, P=0.54) though there was considerable variation, with some jets initiated with the circular fibers at lengths greater than 1.05L_0 (Fig. 2). The muscle lengths at the end of escape jet contraction were significantly shorter for the circular fibers near the inner lumen surface of the mantle than those near the outer surface (t=5.7, P<0.001; Fig. 2). The muscle lengths at the end of

The Journal of Experimental Biology (2014) doi:10.1242/jeb.083907

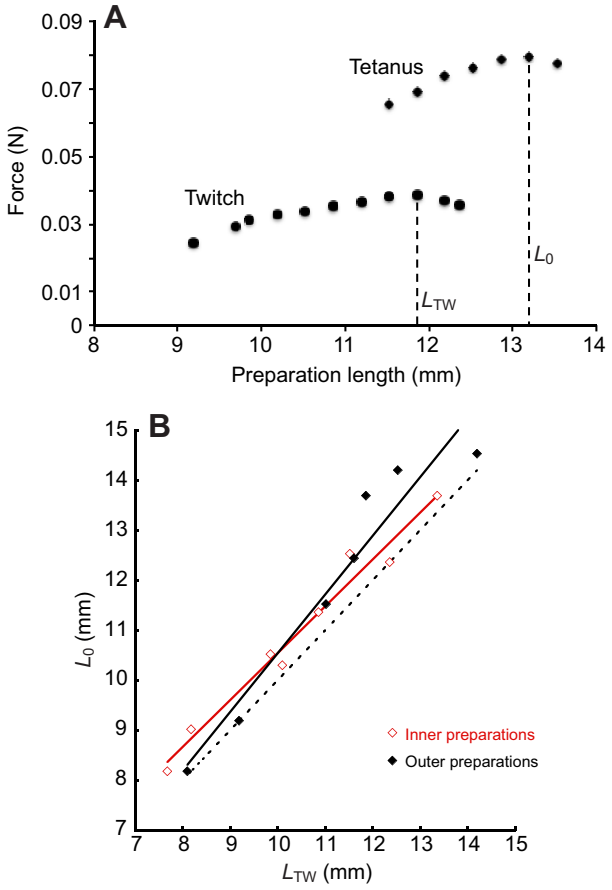

Fig. 4. Effect of stimulus frequency on the length–force relationship. (A) Differences in the length–force relationship for twitch (2 ms pulse width) and tetanic (2 ms pulses, 80 Hz, 100 ms duration) stimulations for a single muscle preparation. (B) The length (L_0) that produced maximum isometric tetanic force versus the length (L_{TW}) that produced the maximum isometric twitch force. Each point represents data from a single preparation. The dashed line intersects the origin and has a slope of 1.0; the solid lines show linear regressions. Inner preparations (open red diamonds): y=0.94x+1.16, R^2=0.97, F=210, P<0.001, n=7; outer preparations (filled black diamonds): y=1.17x–1.19, R^2=0.92, F=68.5, P<0.001, n=6.

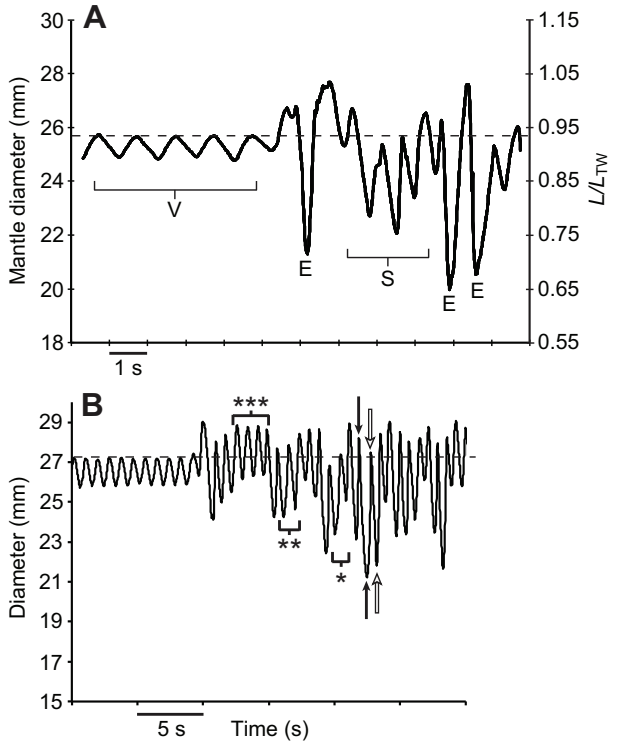

Fig. 5. Unfiltered sonomicrometry records from two squid. (A) Changes in diameter of the outer surface of the mantle along the dorso-ventral midline during ventilatory (V), slow (S) and escape (E) jets from a squid in Group 1. Ventilatory jets occurred when the animals were at rest on the bottom of the tank. The mean velocity of all the slow jets was ≤1 mantle length s^{-1}. The units on the right vertical axis show the mantle diameter changes normalized by L_{TW} for this individual. Mantle diameters that exceeded the mean peak diameter during ventilation (dashed line) were considered to be hyperinflations. The squid hyperinflated during all the escape jets shown but only during two of the slow jets. (B) Diversity of mantle kinematics used in jetting. ***, Three slow jets dominated by hyperinflation of the mantle; **, two slow jets that include modest hyperinflations. The most common pattern seen in slow jetting (*) did not include hyperventilation. The black arrows indicate one escape jet preceded by hyperinflation; this was the most common pattern. The white arrows indicate one escape jet with virtually no hyperinflation.

escape jet contraction were relatively consistent, which may reflect the degree of stereotypy of this behavior.

If the two squid that operated in a hyperinflated state for most of the jets are excluded, the mean operating length ranges of the circular fibers differed significantly at both the start and end of mantle contraction for escape jetting (see Table 1 for statistics).

DISCUSSION

The length–force relationship varies with position in the mantle wall

The length–twitch force and length–tetanic force relationships of the CMP circular muscle fibers varied with radial position in the mantle wall. Consistent with our prediction, the fibers from near the inner surface of the mantle produced higher force, relative to P_0, at all points along the ascending and descending limbs of the length–tension curve than fibers near the outer surface of the mantle.

The mechanism responsible for the transmural difference in length force properties is unknown. Studies of cross-striated muscle fibers have demonstrated that the level of activation can affect the slope of the ascending limb of the length–tension curve (e.g. Rack and Westbury, 1969; Chapple, 1983), with greater activation leading to an increase in the length dependence of force generation (i.e. a steeper slope). We were careful to use a stimulation current that elicited the maximum force for all preparations. In addition, we also explored the possibility that the difference in length–force properties resulted from a difference in length-dependent changes in contraction kinetics of the circular fibers when given a twitch stimulus. Although both T_{max} and $T_{50\%}$ increased slightly with preparation length, there were no significant differences in length-dependent contraction kinetics between the two preparation types. Furthermore, all the circular fibers produced maximum isometric twitch force at a length slightly shorter than the length that produced maximum isometric tetanic force, with no significant differences between the inner and outer preparations. Thus, we conclude that the transmural changes in length–force behavior we report are not an artifact of our experimental approach but instead reflect inherent differences in the circular fibers themselves.

Ultrastructural differences between the CMP circular fibers from near the inner and outer surfaces of the mantle might explain the

The Journal of Experimental Biology (2014) doi:10.1242/jeb.083907

Table 1. Muscle operating length ranges

	Expanded		Contracted	
Jet type	Length	*P*	Length	*P*
Ventilation – outer	0.88±0.091		0.82±0.085	
Ventilation – inner	0.88±0.077		0.83±0.078	
Slow – outer	0.93±0.095	0.04	0.79±0.058	0.02
Slow – inner	0.90±0.13		0.74±0.15	
Escape – outer	0.95±0.095	0.013	0.71±0.064	0.001
Escape – inner	1.0±0.12		0.64±0.067	

Mean (±s.d.) *in vivo* lengths of the circular muscles in the radially expanded mantle at the start of the jet and in the contracted mantle at the end of the exhalant phase of the jet. All values are relative to L_{TW} (the muscle preparation length that generated the maximum isometric twitch force). The data exclude two squid that operated in a primarily hyperinflated state throughout the swimming trials (see Results for details). For slow swimming and escape jetting, the means differed significantly between the inner and outer regions of the mantle (independent-samples *t*-test). The *P*-values for each comparison are indicated. The CMP fibers do not appear to be involved in ventilatory jets, so no statistical tests are included, and the values here are presented merely for comparison with the other jet types. For the ventilation and slow swimming data, the means represent at least 20 jets per squid; the escape jet data were based on seven to 13 jets per squid. *n*=9 animals each for the inner and outer preparations.

ability of the inner fibers to produce higher relative twitch force along the ascending and descending limbs of the length–tension curve. In many striated muscles, long thin and thick filaments and higher thin:thick filament ratios are correlated with higher force output (Jahromi and Atwood, 1969; Josephson, 1975; Granzier et al., 1991). Previous ultrastructural investigations of the circular mantle muscles of squid (Ward and Wainwright, 1972; Moon and Hulbert, 1975; Bone et al., 1981; Thompson and Kier, 2006; Thompson et al., 2008; Thompson et al., 2010b) did not identify transmural differences in myofilament dimensions or their arrangement, but this has not, to our knowledge, been explored in a systematic way.

Intrinsic differences in the CMP fibers might explain the transmural variation in length–force properties. For example, protein-kinase-A-induced phosphorylation of two myofilament lattice proteins (troponin I and myosin binding protein C) in the cardiac myocytes of rats alters the shape of the length–tension curve, increasing the slope of the ascending limb dramatically (Hanft and McDonald, 2010). Expression of different troponin isoforms can also affect force generation in cardiac fibers (Gordon et al., 2000). Recent work has also revealed that the length–force relationship depends on the radial distance between the thin and thick myofilaments (Williams et al., 2013). It is unclear, however, if similar mechanisms to those outlined above occur in the obliquely striated squid mantle muscles.

Squid modulate isometric force and shortening velocity by varying thick filament length, not by expressing different isoforms of myosin heavy chain (Kier and Schachat, 1992; Kier and Schachat, 2008; Thompson et al., 2010b; Shaffer and Kier, 2012). Although other myofilament lattice proteins have the potential to affect the length–force relationship as well (e.g. Hanft and McDonald, 2010), we are currently investigating the dimensions and arrangement of myofilaments in our search for the mechanism driving transmural differences in muscle mechanics. Because we found no significant transmural difference in the maximum isometric tetanic force, we hypothesize that transmural gradients of myosin heavy chain expression or thick filament length do not occur in the mantle CMP circular fibers.

The effects of different length–force relationships on *in vivo* force production

The data are consistent with our hypothesis that the CMP circular muscle fibers near the inner surface produce higher relative forces (both isometric twitch and tetanus) at a given length than the fibers near the outer surface, but the question remains whether the differences in the ascending limb of the length–tension curve are sufficient to allow all of the circular fibers in the mantle to produce similar forces at a given instant during the exhalant phase of the jet. Thompson et al. (Thompson et al., 2010a) showed in *D. pealeii* that the inner surface of the mantle experiences 1.3 to 1.6 times greater circumferential strain than the outer surface at any time point during the exhalant phase of a jet. Because circular fibers are oriented in transverse planes of the mantle and also appear to follow a perfectly circumferential trajectory, there are no architectural specializations, such as those found in mammalian cardiac ventricle muscle (Lunkenheimer et al., 2004; Anderson et al., 2006; Anderson et al., 2009) or vertebrate skeletal muscles (Alexander, 1969; Rome and Sosnicki, 1991; Wakeling and Johnston, 1999; Azizi et al., 2008) that could permit all of the fibers to experience approximately the same range of strains during jetting. Thus, the transmural gradient of circumferential strain in the mantle may require muscle fibers from the inner surface to operate farther left on the ascending limb of the length–tension curve at any instant during mantle contraction. But if the length–tension curve for the fibers from near the inner surface has a lower slope and higher *y*-intercept than the fibers from the outer surface of the mantle, then all of the circular fibers might produce approximately the same force at a given instant in the contraction cycle. This assumes that all of the CMP circular fibers are activated to a similar extent, which has not yet been established. How different must the slope and intercept be to allow this to happen?

The question can be addressed as follows. First, Thompson et al. (Thompson et al., 2010a) recorded circumferential strain simultaneously from both the inner and outer surfaces of the mantle from 12 *D. pealeii* that were similar in size [mean ± s.d. dorsal mantle length (DML)=157±44 mm] to the ones used in the present study. We fit a linear regression to their circumferential strain data that allowed us to predict the circumferential strain experienced by the inner surface of the mantle for a given strain at the outer surface (Fig. 6). Next, we used the sonomicrometry data for the outer surface of the mantle from the present study with the regression equation (Fig. 6) to estimate the corresponding circumferential strain at the inner lumen surface. Finally, we normalized those calculated strain data for the inner surface of the mantle by L_0 and plotted them on the length–twitch force curve (from Fig. 1A) and length–tetanic force curve (from Fig. 2). This allowed us to estimate the operating length range of the inner circular fibers relative to the outer fibers at any single point on the length–tension curve and, thus, predict the twitch or tetanic force output required by the inner fibers to match that of the outer fibers at a given instant in time.

The results of this analysis are shown in Fig. 7. The predicted lengths of the circular muscle fibers (relative to L_0) near the inner surface of the mantle fall very close to the actual ascending limb of the length–tension curve for the inner muscle preparations. Thus, we hypothesize that the differences in slope and intercept between the two length–tension curves may allow all of the CMP muscle fibers in the mantle to produce approximately the same force at any instant in the contraction cycle. Unfortunately, we do not know how much stress the CMP circular fibers from each location produce *in vivo* and cannot test this hypothesis at this time. This analysis is also complicated by potential transmural differences in (1) fiber

The Journal of Experimental Biology (2014) doi:10.1242/jeb.083907

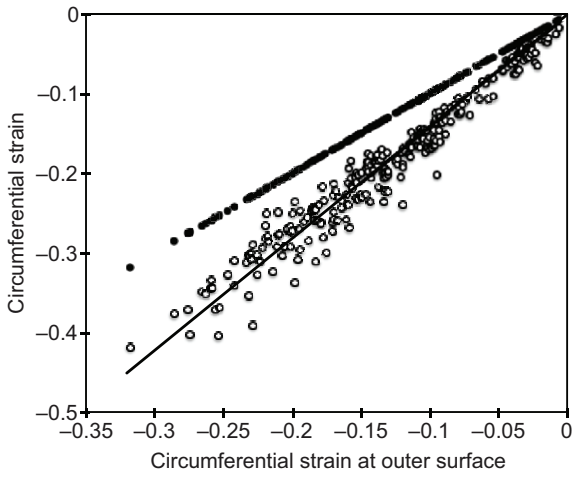

Fig. 6. Circumferential strain of the outer (filled symbols) and inner (open symbols) surfaces of the mantle as a function of circumferential strain at the outer surface of the mantle. Negative values arbitrarily indicate contraction of the mantle and shortening of the circular fibers. The linear regression was constrained to pass through the origin ($F_{1,286}$=4228, P<0.001; y=1.37x, adjusted R^2=0.936). Sample size: 288 jets from nine adult *D. pealeii*. Data are from Thompson et al. (Thompson et al., 2010a).

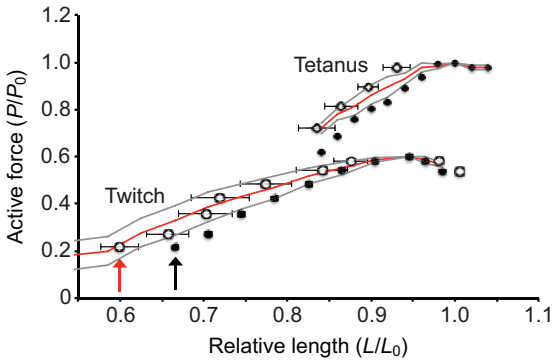

Fig. 7. Predicted muscle lengths. The filled symbols show the mean length–twitch force and length–tetanic force relationships for the circular fibers from near the outer surface of the mantle (from Fig. 1A and Fig. 2). Each filled symbol is associated with an open symbol to the left (ascending limb) that represents the mean ± s.d. predicted muscle length for the circular fibers from the inner surface of the mantle. For example, when the circular fibers near the outer surface of the mantle reach 0.67L_0 (black arrow) during mantle contraction, the circular fibers from near the inner surface are predicted to be at 0.60L_0 (red arrow) at the same instant in time. The red (mean) and gray (s.d.) lines show the mean length–force curves for the circular fibers from near the inner surface of the mantle (from Fig. 1A and Fig. 2). See Discussion for details.

activation, (2) the force–velocity properties of the circular fibers, and (3) shortening velocity *in vivo* (see Thompson et al., 2010a). These issues will be the subjects of future studies. In addition, we intend to characterize the force–velocity relationships and measure work output in preparations subjected to simulated *in vivo* patterns of stimulation and length change.

Circular muscle fiber operating length range

The CMP circular muscle fibers operated primarily on the ascending limb of the length–tension curve. They functioned routinely over muscle lengths at which force output ranged from only 85% to 40% of P_0, and during escape jets from 100% to approximately 30% of P_0. The operating length range of the muscles does not, therefore, appear to optimize work output. Shifting the range of operating lengths 0.15L_0 to the right on the length–tetanic force curve would center the length ranges on the force maximum region and, for most jets, likely result in higher work output (see Burkholder and Lieber, 2001). This finding is suggestive of a trade-off, but the nature of that trade-off is not yet clear.

One strong possibility is that squid trade muscle work output for maximum force production during escape responses. Squid use both the mantle and the fins for locomotion: adult animals use their fins extensively for station-holding and slow swimming, combinations of the fins and jetting for slow swimming and faster cruising, and the jet exclusively for escape responses (Bartol et al., 2008; Bartol et al., 2009). In two other species of loliginid squid (*D. opalescens* and *Lolliguncula brevis*), the thin layers of superficial mitochondria-rich (SMR) circular fibers provide power for ventilation and slow swimming while the CMP circular fibers we investigated are used periodically to augment power during slow swimming and also provide power for the escape jets (Gosline et al., 1983; Bartol, 2001). Because they operate on the ascending limb, the hyperinflation that precedes most escape jets lengthens the circular fibers close to L_0, thus allowing them to produce maximum force at the onset of the escape response.

There are several other examples of animals whose muscles operate solely along the ascending limb of the length–tension curve while providing power for locomotion or the pumping of fluid, situations in which maximizing work output might seem to be favored. The cross-striated adductor muscle of the bay scallop *Argopecten irradians* operates almost entirely on the ascending limb during the valve clapping movements required for swimming (Olson and Marsh, 1993; Marsh and Olson, 1994), as does the synchronous wing depressor of the hawkmoth *Manduca sexta* during flight (Tu and Daniel, 2004) and the human soleus muscle during walking and running (Rubenson et al., 2012). The papillary muscles of mammals (Allen and Kentish, 1985; Layland et al., 1995) and the atrial trabeculae of frogs (Winegrad, 1974) also operate solely along the ascending limb.

Operating on the ascending limb allows cyclically active muscles to respond to a stretch by increasing their capacity to produce force, though at the cost of decreased work and power. Such a response is hypothesized to provide non-neuronal mechanisms for regulating muscle excursion lengths during cyclical contractions (Tu and Daniel, 2004; Rubenson et al., 2012). The circular mantle muscles of squid are similar to the cardiac, flight and adductor muscles in that they contract and elongate rhythmically during locomotion and ventilation, and the degree of muscle lengthening during mantle cavity refilling can vary widely. But the cardiac, flight and adductor muscles have much steeper ascending limbs than the mantle fibers of squid, and thus force output is much more sensitive to changes in muscle length. Thus, we hypothesize that the observed operating length range of the mantle fibers may be more important for maximizing thrust during the initial phase of the escape jet than for regulation of muscle excursion length.

Length-dependent contraction kinetics and the effect of stimulus frequency on the length–force relationship

Both the leftward shift in the peak of the length–tension curve as stimulus frequency increases and the length dependence of activation of cross-striated skeletal and cardiac fibers in an isometric twitch are well-known phenomena (e.g. Rack and Westbury, 1969; Malamud, 1989; Roszek et al., 1994; Brown et al., 1999) that are assumed to be characteristic of striated fibers. In length-dependent

activation in vertebrate striated fibers, the time to maximum isometric twitch force and the 50% relaxation time both increase significantly as fiber length increases (Rack and Westbury, 1969). The mechanisms responsible are still debated, with evidence suggesting roles for Troponin C (Babu et al., 1988; but see McDonald et al., 1995), Troponin I (Arteaga et al., 2000), Titin (Fukuda et al., 2001; Fukuda et al., 2003; Terui et al., 2008), and lateral/radial spacing of the thick and thin filaments (McDonald and Moss, 1995; Williams et al., 2013).

The CMP circular muscles exhibited a rightward shift in the peak of the length–force relationship as stimulus frequency increased (Figs 2, 4). They also showed no evidence of length-dependent changes in contraction kinetics (i.e. length-dependent activation) in an isometric twitch (Fig. 3). These differences are intriguing and may imply fundamental differences in the intrinsic properties of the obliquely striated circular fibers compared with cross-striated skeletal and cardiac fibers. The muscles of many invertebrates, including squid, have myosin-linked regulation. In these muscles, initiation of crossbridge cycling occurs via binding of Ca^{2+} to the essential light chain of myosin (Xie et al., 1994; Fromherz and Szent-Györgyi, 1995; Houdusse et al., 1999; for a review, see Szent-Györgyi, 2007). If length-dependent activation in vertebrate striated fibers involves changes in a troponin- or titin-linked mechanism, myosin-linked regulation may explain the absence of length-dependent changes in contraction kinetics during isometric twitches in the mantle circular fibers.

Twitch:tetanus ratio

Milligan et al. (Milligan et al., 1997) and Thompson et al. (Thompson et al., 2008) reported a threefold lower twitch:tetanus ratio for the CMP circular muscle fibers than we report here. A difference in excitation–contraction coupling between the species may account for this disparity in the case of Milligan et al. (Milligan et al., 1997) because they studied *Alloteuthis subulata*, but Thompson et al. (Thompson et al., 2008) also studied *D. pealeii*. We noted in the present study that P_{TW} dropped steadily as the preparations first started to fatigue, while P_0 remained constant. Monitoring preparation health through periodic isometric tetanic contractions, as Thompson et al. (Thompson et al., 2008) did, would not allow the decline in P_{TW} to be detected. Thus, we feel the twitch:tetanus ratio reported here for *D. pealeii* may be more reliable than that reported previously by Thompson et al. (Thompson et al., 2008).

The evolution and functional diversity of obliquely striated muscles

Obliquely striated muscles, so-called because the dense bodies (i.e. Z-elements) are aligned at an oblique angle to the long axis of the cell, have been reported in members of at least 14 different invertebrate phyla: Annelida (e.g. Rosenbluth, 1968), Brachiopoda (Kuga and Matsuno, 1988), Bryozoa (Bouligard, 1966), Echinodermata (Candia Carnevali et al., 1986), Gastrotricha (Rieger et al., 1974; Teuchert, 1974), Gnathostomulida (Rieger and Mainitz, 1977); Mollusca (e.g. Amsellem and Nicaise, 1980; Matsuno and Kuga, 1989), Nematoda (e.g. Rosenbluth, 1965), Nematomorpha (Eakin and Brandenburger, 1974; Lanzavecchia et al., 1979) Nemertea (Norenburg and Roe, 1998), Platyhelminthes (MacRae, 1965; Ward et al., 1986), Rotifera (Bouligard, 1966), Sipunculida (DeEguileor and Valvassori, 1977) and Urochordata (Bone and Ryan, 1974). Obliquely striated fibers are ubiquitous in some of these phyla (e.g. Nematoda), but are restricted in their distribution in others (e.g. the Mollusca, Urochordata and Sipunculida). A careful analysis of the evolution of these muscles is needed, but mapping the distribution onto a recent eumetazoan phylogeny (Paps et al., 2009) suggests that oblique striation evolved independently several times.

Such putative parallel evolution implies that the mechanical properties of obliquely striated muscles may be much more diverse than has been assumed (for reviews, see Rosenbluth, 1972; Toida et al., 1975; Lanzavecchia, 1977). For example, Lanzavecchia and colleagues (Lanzavecchia and De Eguileor, 1976; Lanzavecchia, 1977; Lanzavecchia and Arcidiacono, 1981) proposed that obliquely striated fibers are specialized to produce relatively high forces at exceptionally long muscle lengths. Using leeches as a model, they provided morphological evidence that overlap between the thick and thin filaments of the longitudinal body wall muscles is maintained over a fivefold increase in body length. Gerry and Ellerby (Gerry and Ellerby, 2011) showed recently that the longitudinal fibers of the body wall of the medicinal leech (*Hirudo verbena*) operated solely on the descending limb of the length–tension curve at very long muscle lengths during swimming and feeding. In the presence of serotonin, the longitudinal fibers produced relatively high forces ($\geq 0.5P_0$) at muscle lengths of nearly $2.5L_0$.

In contrast, the present study shows that the obliquely striated CMP mantle fibers of squid operate almost exclusively on the ascending limb of the length–tension curve. Moreover, investigations of the length–force relationships of obliquely striated muscles in earthworms (Hidaka et al., 1969; Tashiro and Yamamoto, 1971), the horse leech *Haemopis sanguisuga* (Miller, 1975), and squid and cuttlefish (Milligan et al., 1997; Kier and Curtin, 2002) showed that these muscles produce force over a moderate range of lengths *in vitro* (Table 2), observations inconsistent with the hypothesis that oblique striation is a specialization for producing relatively high forces at long muscle lengths.

Furthermore, it is likely that considerable undescribed mechanical diversity exists among obliquely striated muscles, not only among different animals but also among different muscles in the same individual. For example, the tentacles of *D. pealeii* are elongated by 80% or more during prey capture (Kier, 1982) and then shorten to bring the prey within grasp of the arms, thereby requiring the obliquely striated longitudinal muscle fibers (Kier, 1985) that retract the tentacles to operate over a wide range of muscle lengths. In contrast, the obliquely striated funnel retractor muscle in the same animal experiences only small changes in length (±5%) during jetting, and operates nearly isometrically during the exhalant phase of the jet (Rosenbluth et al., 2010). In addition, the obliquely striated transverse muscle fibers of the arms of two squid species (*D. pealeii* and *Sepioteuthis sepioidea*) experience virtually no change in length while providing support for bending movements (Kier, 1982). To better understand the evolution and functional implications of oblique striation, investigations of the contractile properties and *in vivo* operating length ranges of obliquely striated muscles both from a broader taxonomic range and also from functionally diverse muscles within individuals is needed.

MATERIALS AND METHODS

Overview of experiments

The experiments were conducted over three consecutive summers, with data collection each summer focusing on different aspects of muscle physiology or *in vivo* muscle function. In the summer of 2011, we used sonomicrometry to measure circumferential strain of the inner and outer surfaces of the mantle during jet locomotion as the first step in the investigation of the *in vivo* operating length ranges of the circular muscles. As the second step in this investigation, and also to evaluate the hypothesis that the length–force

The Journal of Experimental Biology (2014) doi:10.1242/jeb.083907

Table 2. Length–force properties of obliquely striated muscle preparations

Species	Muscle	Range of lengths that produced ≥0.5P_0
Pheretima communissima	Longitudinal body wall muscle	0.75L_0 to 1.42L_0[a]
		0.67L_0 to 1.11L_0[b]
	Circular body wall muscle	0.84L_0 to 1.09L_0[b]
Haemopis sanguisuga[c]	Longitudinal body wall muscle	0.52L_0 to 1.17L_0[c]
Hirudo verbana[d]	Longitudinal body wall muscle	0.67L_0 to 2.52L_0[d,*]
Alloteuthis subulata	Circular mantle muscle	0.64L_0 to 1.37L_0 (twitch)[e,‡]
Sepia officinalis	Transverse muscle of the arm	0.67L_0 to 1.33L_0 (brief tetanus)[e,‡]
Doryteuthis pealeii	Circular mantle muscle	0.69L_0 to 1.22L_0 (brief tetanus)[e,‡]
		0.70L_0 to 1.1L_0 (twitch, inner fibers)[f,‡]
		0.77L_0 to 1.1L_0 (twitch, outer fibers)[f,‡]
	Transverse muscle of the arm	0.71L_0 to 1.09L_0 (twitch)[g,‡]

Length–force relationships for the obliquely striated muscles of an earthworm (*P. communissima*), two leeches (*H. sanguisuga* and *H. verbena*) and three cephalopods (*A. subulata*, *S. officinalis* and *D. pealeii*). The values were measured from published length–tension curves. L_0, muscle preparation length that generated the maximum isometric tetanic force; P_0, peak isometric tetanic force.

[a]Tashiro and Yamamoto (Tashiro and Yamamoto, 1971).

[b]Hidaka et al. (Hidaka et al., 1969).

[c]Miller (Miller, 1975).

[d]Gerry and Ellerby (Gerry and Ellerby, 2011).

[e]Milligan et al. (Milligan et al., 1997).

[f]Present study.

[g]Kier and Curtin (Kier and Curtin, 2002).

*The lowest force reported on the ascending limb was 0.73P_0.

‡The values for the descending limb represent the longest preparation lengths reported by the authors. In all cases, the forces were higher than 0.5P_0.

relationships of the circular muscle fibers vary transmurally, we used *in vitro* tests to measure the length–twitch force relationship of the circular muscle. Although the CMP circular fibers that were the focus of our study appear to be stimulated in brief tetanus *in vivo* (Gosline et al., 1983; Bartol, 2001), we used a twitch stimulus because it greatly increased the longevity of the preparations (relative to tetanic stimulation) and improved the odds of a successful experiment. This was crucial because we needed both sonomicrometry and muscle mechanical data from the same individual in order to identify the operating length ranges of the circular fibers.

Using twitch stimulations for the muscle preparations required additional experiments to ensure that any transmural differences in the length–twitch force relationship we observed were not merely artifacts of our experimental approach. Thus, in the summers of 2012 and 2013 we investigated the possibility that length-dependent activation of the CMP circular muscle preparations differed transmurally. This step was necessary because the cross-striated fibers of vertebrates and at least some arthropods exhibit greater activation at long lengths when stimulated with a single pulse of current (e.g. Rack and Westbury, 1969; Malamud, 1989; Roszek et al., 1994). If the circular muscles of squid exhibited length-dependent changes in contraction kinetics, and if those kinetics varied transmurally, then our comparisons of the length–twitch force relationship would have been inappropriate. In 2012 and 2013 we also performed experiments to measure the length–tetanic force and length–twitch force relationships in the same CMP circular muscle preparations. These experiments allowed us to correlate the length–tetanic force relationship with the sonomicrometry results, which as described above, required twitch stimulation for the viability of the preparations. In addition, we measured the twitch:tetanus ratio of the CMP fibers.

Animals

We used squid jigs and cast nets to capture adult *D. pealeii* from lighted piers and docks in Boothbay Harbor and South Bristol, Maine, USA, during the summers of 2011 (Group 1 squid), 2012 (Group 2) and 2013 (Group 3). The animals were transported to the laboratory in 20 l buckets and maintained in a 500 l aquarium supplied with flow-through seawater. Water temperature in the aquarium was 15 to 17°C. The animals were fed small fish (*Brevoortia tyranus* and *Menidia menidia*) daily until used in the experiments. Most squid were maintained in the laboratory for only a few days.

Group 1 included 20 squid used for measuring both the *in vivo* operating length range and length–twitch force relationship of the circular muscles from near the outer surface (n=10, 143±37 mm, mean ± s.d. DML) and the inner surface (n=10, 161±37 mm) of the mantle. Group 2 was composed of 16 squid (194±34 mm DML) for measurements of the twitch:tetanus ratio of the circular fibers, and Group 3 included 10 squid (150±55 mm DML) for evaluating length-dependent changes in contraction kinetics, the twitch–tetanic force relationship, and maximum isometric stress of the circular fibers. Note that in some cases for the squid in Groups 2 and 3, we were able to measure the contractile properties of the circular fibers from the inner and outer surface from the same individual, while in other individuals we were able to measure the properties of fibers from only one surface. Thus, the sample sizes for the twitch:tetanus ratio, twitch–tetanic force relationship, length-dependent contraction kinetics and maximum isometric stress experiments do not necessarily equal the number of individuals in the two sample population groups. The sample sizes for each experiment are listed in the Results.

Sonomicrometry

We used sonomicrometry to measure circumferential strain of the inner and outer surfaces of the mantle during jet locomotion. We anesthetized squid in cold seawater (3 to 5°C) (O'Dor and Shadwick, 1989; Bower et al., 1999) and surgically affixed 1 mm diameter sonomicrometry transducers (Sonometrics Corp., London, ON, Canada) to the mantle. The transducers were attached to the mantle within a single transverse plane approximately one-third of the DML from the anterior edge (Fig. 8A,B). We chose this location because it experiences the largest amplitude changes in diameter during jetting. For experiments that focused on the outer surface of the mantle, transducers a and c (Fig. 8B) were sutured (6/0 polypropylene) to the outer surface of the mantle at the dorsal and ventral midlines, respectively. For experiments that focused on the inner surface of the mantle, transducer a was sutured to the outer surface of the mantle at the dorsal midline and transducer b was glued to the inner lumen surface of the mantle at the ventral midline with a drop of cyanoacrylate (Vetbond, 3M, St Paul, MN, USA) (Fig. 8B). All of the leads were secured to the dorsal collar of the mantle with a surgical staple to reduce interference with the mantle and fins during swimming.

Following surgery, the squid were transferred to a narrow tank (1.3×0.3×0.3 m deep) filled with natural seawater at 15–17°C. Each animal recovered quickly and then swam mantle-first and arms-first at various speeds using combinations of jetting and fin movement. We recorded sonomicrometry data at 150 Hz during swimming. The most rapid escape jets we recorded had exhalant phases of approximately 0.15 s and inhalant

The Journal of Experimental Biology (2014) doi:10.1242/jeb.083907

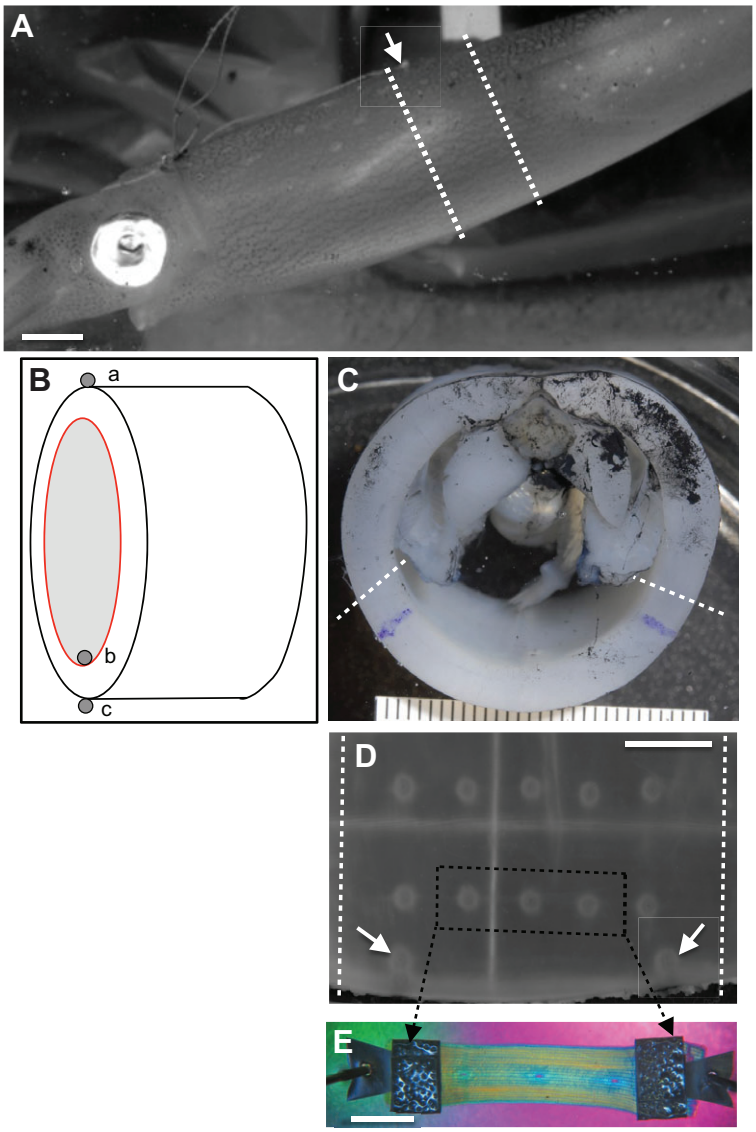

Fig. 8. Outline of methods used to relate *in vivo* muscle operating length range to the length–force relationship. (A) Photograph of an individual *D. pealeii* during a swimming trial. One of the sonomicrometry crystals is visible at the dorsal midline (arrow); the other is glued to the inner lumen surface at the ventral midline and is hidden from view. The sonomicrometry leads are visible above the head. Dashed lines show approximately where a ring of mantle tissue was excised post mortem. Scale bar, 1 cm. (B) Mantle ring schematic to show placement of the sonomicrometry crystals (a, b and c; gray filled circles). The red line marks the inner lumen surface of the mantle; the black lines the outer surface. (C) Photograph of a ring of mantle tissue. Dorsal midline is at the top of the photo, and squid ink stains a portion of the dorsal mantle wall. The blue lines are the reference marks made by a surgical marking pen. We measured the circumference of the inner or outer surface of the mantle and the corresponding arc length of the inner or outer surface between the blue reference marks, and then cut the ring at the two dashed lines. The resulting slab of tissue was then glued, outer or inner surface down (depending on the experiment), to the stage of the vibratome. Millimeter ruler serves as scale bar. (D) Photograph of the slab of mantle tissue glued to the vibratome stage. The white vertical and horizontal lines are part of the stage, and are visible through the transparent mantle tissue. We made reference holes by perforating the slab with a fine insect pin. The two holes indicated by the white arrows are directly over the reference marks made by the tissue pen. The remaining holes follow the trajectories of bands of circular muscle fibers. We used a vibratome to cut 300 µm thick sheets from the slab of tissue, and the appropriate sheet (see Materials and methods for details) was further dissected to make a muscle preparation. The dashed lines indicate the location of the preparation. (E) Photograph (polarized light microscopy with first-order red filter) of a preparation with foil clips attached and pinned out after a length–force experiment at L_{TW}. The reference holes are visible on the midline of the preparation. Scale bars in D and E, 5 mm.

phases of approximately 0.4 s; thus, the two phases were described by a minimum of 30 and 90 data points, respectively. We positioned a digital video camera (Flip Ultra HD, 1280×720 pixel resolution, 30 frames s^{-1}) to record lateral views of the squid as they jetted. We used the video records to help select appropriate sequences for analysis. The duration of most swimming trials was 10 min. At the end of the trial, we euthanized the squid and evaluated the alignment of the transducers.

Sonomicrometry data analysis

The CMP circular fibers of squid provide power for the escape jet and are also active sporadically during slow swimming (Gosline et al., 1983; Bartol, 2001). We analyzed sequences only in which the squid performed vigorous escape jets.

The sonomicrometry transducers recorded changes in the diameter of the outer or inner surfaces of the mantle at a single transverse plane along the dorso-ventral midline (Fig. 8B). The diameter of the outer surface was measured directly from the sonomicrometry traces. Calculation of the diameter of the inner surface required that we take into account the thickness of the dorsal mantle wall. Because the mantle remains circular in cross-section during jetting (Ward, 1972; Gosline and Shadwick, 1983), we used the diameter data to calculate the instantaneous circumference of either the inner lumen or outer surface of the mantle. We corrected the sonomicrometry data to account for transducer diameter and their location on the surface of the mantle by subtracting 1.0 mm from, or adding 1.0 mm to, the diameters recorded for experiments that focused on the outer or inner surfaces of the mantle, respectively.

Length–twitch force experiments

Immediately after the end of a sonomicrometry experiment, the animal was anesthetized in cold seawater, and then decapitated. We cut a transverse ring of mantle tissue that included the sonomicrometry crystals (Fig. 8A,B), removed the skin, and placed the ring in a bath of chilled (3.5°C) modified artificial seawater solution containing (in mmol l^{-1}): NaCl (450), $MgCl_2 \cdot 6H_2O$ (10), Hepes (10) and EGTA (10), pH adjusted to 7.8 with 2 mol l^{-1} NaOH (Milligan et al., 1997). We assessed the accuracy of the sonomicrometry crystal placement, detached them, and then used a surgical pen to draw two widely spaced marks on the cut surface of the ventral side of the ring (Fig. 8C). We photographed the ring and used morphometrics software to measure the circumference of either the inner or outer surface of the mantle, depending on the placement of the sonomicrometry crystals. We also measured the arc length of the inner or outer surface between the reference marks (Fig. 8C). These measurements allowed us to relate the relevant arc length between the marks to the circumference of the inner or outer surface of the mantle ring.

We next removed the ventral region of the ring that included the two reference marks and glued it with Vetbond, outer surface or inner surface down (depending on the experiment), to the stage of a vibratome (Fig. 8D). Experiments on the inner surface and the outer surface were interspersed

over time. The vibratome bath was filled with chilled modified artificial seawater and maintained at 3.5°C. We then pierced the slab with an insect pin, forming a series of small but visible holes in the following locations: (1) one hole at the location of each mark of the tissue pen and (2) two straight lines of evenly spaced holes (Fig. 8D). We took care to ensure that each line of holes followed the trajectory of a single band of circular fibers.

We used the vibratome to cut 300 µm thick sheets of mantle tissue. The vibratome sliced through the radial muscle fibers, thereby inactivating them (see Milligan et al., 1997; Thompson et al., 2008; Thompson et al., 2010b). We selected a sheet that was 300 µm away from the appropriate surface of the mantle (i.e. inner or outer, depending on the experiment). This position insured that no SMR circular muscle fibers (see Preuss et al., 1997; Bone et al., 1981; Mommsen et al., 1981), which occur in layers within approximately 200 µm of both the inner and outer surfaces of the mantle of *D. pealeii* (Thompson et al., 2008), were present in the preparations. Thus, our preparations were composed of the CMP (see Preuss et al., 1997) muscle fibers, and remnants of radial fibers and collagenous connective tissue fibers. We further dissected the sheet into a preparation 10–12 mm long by 4–5 mm wide, with the line of holes in the center of each preparation (Fig. 8D). The ends were glued to T-shaped aluminum foil clips with Vetbond (Fig. 8E). Each muscle preparation had two or three of the pinholes visible between the foil clips.

The muscle preparation was transferred to a bath filled with 100 ml of cold (3.5°C) standard artificial seawater solution containing (in mmol l^{-1}): NaCl (470), KCl (10), $CaCl_2$ (10), $MgCl_2 \cdot 6H_2O$ (50), glucose (20) and Hepes (10), pH adjusted to 7.8 with 2 mol l^{-1} NaOH (Milligan et al., 1997). After 60 min in the bath, we transferred the preparation to a recirculating temperature-regulated bath filled with standard artificial seawater at 15°C and attached one end to a fixed hook and the other to a hook on a muscle lever system (300B, Aurora Scientific Inc., Aurora, ON, Canada).

The muscle preparations were subjected to a twitch stimulus with rectangular constant current pulses (0.002 s pulse width) via platinum foil electrodes that were of sufficient size to cover the preparation. Prior to starting the length–twitch force experiments, we first determined the current amplitude that activated the preparation maximally. Interestingly, supramaximal stimulation consistently caused a decrease in force output.

We began each length–force experiment with the preparation barely slack and lengthened it as the experiment continued. Each length–tension curve was composed of 13 to 15 points. At the end of the experiment, we adjusted the preparation length to L_{TW} (i.e. the preparation length at peak isometric twitch force), stimulated it again to ensure that peak isometric force was stable (if it decreased by more than 10%, the animal was excluded from the study), and then measured the distance between the pinholes (Fig. 8E). The distance between the pinholes at L_{TW} was used to relate length–force data to the sonomicrometry data (see below).

Relating the sonomicrometry data to the length–tension curve

Estimating the operating length ranges of the muscle fibers in the mantle is challenging because, like many other soft-bodied invertebrates, there are no landmarks that can be used to relate muscle lengths to body or appendage kinematics. Measuring muscle strain directly by inserting sonomicrometry crystals into the tissue is similarly challenging because (1) the mantle is circular in cross-section and the crystals measure straight-line distances, and (2) the large changes in mantle circumference during jetting preclude close spacing of the crystals to help reduce errors due to mantle geometry. Therefore, we used the reference marks and pin holes described above (Fig. 8C–E) to relate L_{TW} to mantle circumferential strain as follows. First, we calculated the ratio of the arc length between the pen marks to the circumference for either the inner or outer surface (depending on the experiment) of the mantle rings. Next, we measured the spacing between the two pinholes on the slab that were located adjacent to the two pen marks (the spacing changed as we flattened the slab and glued it to the stage) and calculated the 'slab circumference' using the aforementioned ratio. Next, we divided the measured distance between the pinholes at L_{TW} by the measured distance between the same pinholes in the slab of mantle tissue glued to the vibratome stage. We referred to this as the L_{TW}/L_{Slab} ratio. By multiplying the 'slab circumference' by the L_{TW}/L_{Slab} ratio, we were then able to determine the circumference of the relevant surface of the mantle at L_{TW}. We then used that circumference to normalize the sonomicrometry data by L_{TW}.

Length-dependent contraction kinetics and length–tetanic force relationship of the circular fibers

In the striated fibers of vertebrates and arthropods, the degree of fiber activation varies with length when preparations are activated with a twitch stimulus (e.g. Rack and Westbury, 1969; Malamud, 1989; Roszek et al., 1994). Transmural differences in such length-dependent contraction kinetics, if present, might affect the length–twitch force relationship of the outer or inner CMP circular mantle fibers given that we used a twitch stimulus. Thus, we investigated potential differences in length-dependent contraction kinetics of the circular fibers in two ways as follows. From the length–twitch force data collected from the animals in Group 1, we first compared the time required (T_{max}) for force to rise from the onset of stimulation to the peak as preparations were lengthened from their shortest to their longest lengths. We made similar comparisons for the time required ($T_{50\%}$) for force to fall from the maximum to 50% of the maximum. We then performed linear regressions of preparation length versus T_{max} and, separately, versus $T_{50\%}$. We used independent-samples *t*-tests to compare the slopes and *y*-intercepts of the regressions between preparations from the outer and inner surfaces of the mantle.

We also examined length-dependent activation by comparing the preparation lengths that generated maximum isometric twitch force (L_{TW}) and maximum isometric tetanic force (L_0). We anesthetized the squid in Group 3 in chilled seawater and prepared muscle preparations as described for the length–twitch force experiments above, though we did not perforate the preparations with a pin. We determined the current amplitude needed to activate the preparations maximally and then performed length–twitch force experiments to determine the length–tension curve using a twitch (2 ms pulse width) stimulus. We adjusted the preparation length to $0.84L_{TW}$ and then performed length–force experiments using tetanic (0.002 s pulse width, 80 Hz, 0.1 s duration) stimulation.

Performing the twitch stimulation experiments before the tetanic stimulation experiments allowed us to find the zone of highest forces of the preparation more rapidly and with less fatigue, which was necessary for viability of the preparations. In several preparations we rechecked the twitch results following the tetanic stimulation series to confirm that the length–force relationship was unchanged. We thus do not believe that conducting the twitch stimulations first introduced a bias, but preparation viability did not allow us to reverse the order.

Following these experiments, we fixed (3.75% formaldehyde in seawater) the preparations at L_0, embedded them in glycol methacrylate plastic (GMA, Technovit 7100, Heraeus Kulzer GmbH, Wehrheim, Germany), cut 7 µm sections transverse to the long axes of the circular fibers, and stained the sections in Picrosirius modified for use in GMA (Cerri and Sasso-Cerri, 2003). GMA plastic was chosen because it minimizes dimensional changes during embedding and sectioning procedures. We then used morphometrics software (Sigma Scan, Systat Software, Inc., San Jose, CA, USA) to measure the physiological cross-section of the circular muscle fibers of the preparations from photomicrographs of the sections. The inactivated radial muscle fibers were excluded from the area measurement because they do not contribute to force production by the preparation. The physiological cross-section measurements allowed us to calculate the maximum isometric stress for both twitch (P_{TW}) and tetanic (P_0) stimuli. We used independent-samples *t*-tests to compare P_0 and also differences in L_{TW} versus L_0 for the preparations.

Determination of twitch:tetanus ratio

We anesthetized the squid in Group 2 in chilled seawater and decapitated them, as described above. We then removed large blocks (15×20 mm) of the mantle tissue near the ventral midline one-third to one-half of the DML from the anterior margin of the mantle and used the vibratome to prepare 300 µm thick preparations as described above. We determined the current amplitude needed to activate the preparations maximally with a twitch stimulus (2 ms pulse width) and then performed stimulus frequency–force experiments. In five animals, we determined that maximum tetanic force was produced at 80 or 100 Hz (0.002 s pulses, 0.1 s tetanus duration). In all subsequent experiments, we cycled our stimulation protocol from twitch to 80 to 100 Hz (with 5 min rest periods between stimulations) until the twitch and tetanic force stabilized. We reported the twitch:tetanus ratio only when the twitch force was stable for two consecutive trials. Remarkably, the twitch:tetanus

ratio changed very little, even as the twitch force generated by a preparation increased over successive initial trials and then stabilized.

Statistics

The data from each group of squid were distributed normally. We used independent-samples *t*-tests and linear regression analysis as noted in the Results. All statistical comparisons were performed with SPSS 19 (IBM, Armonk, NY, USA).

Acknowledgements

We thank Harry Perilstein and Natalie Friedman for help with the muscle mechanics and sonomicrometry experiments, Jessica Kurth for assistance with the histology and morphometrics, and Dr Kevin Eckelbarger, Timothy Miller and Linda Healy at the Darling Marine Center for providing housing, laboratory space and aquaria for the squid. We thank Cole Natale and Ian, Claire and Sophie Thompson for help in capturing and caring for the squid.

Competing interests

The authors declare no competing financial interests.

Author contributions

The project was conceived by J.T.T. and W.M.K. All three authors participated in the planning and execution of the experiments, and in the subsequent analysis and interpretation of the data. J.T.T. wrote the first draft of the manuscript and all of the authors revised it.

Funding

The National Science Foundation provided support via a collaborative grant to J.T.T. [IOS-0950827] and to W.M.K. [IOS-0951067]. We thank two anonymous reviewers for helpful comments.

Supplementary material

Supplementary material available online at
http://jeb.biologists.org/lookup/suppl/doi:10.1242/jeb.083907/-/DC1

References

Alexander, R. M. (1969). The orientation of muscle fibres in the myomeres of fishes. *J. Mar. Biol. Assoc. U. K.* **49**, 263-289.
Allen, D. G. and Kentish, J. C. J. (1985). The cellular basis of the length-tension relation in cardiac muscle. *J. Mol. Cell. Cardiol.* **17**, 821-840.
Amsellem, J. and Nicaise, G. (1980). Ultrastructural study of muscle cells and their connections in the digestive tract of *Sepia officinalis*. *J. Submicrosc. Cytol.* **12**, 219-231.
Anderson, R. H., Ho, S. Y., Sanchez-Quintana, D., Redmann, K. and Lunkenheimer, P. P. (2006). Heuristic problems in defining the three-dimensional arrangement of the ventricular myocytes. *Anat. Rec.* **288A**, 579-586.
Anderson, R. H., Smerup, M., Sanchez-Quintana, D., Loukas, M. and Lunkenheimer, P. P. (2009). The three-dimensional arrangement of the myocytes in the ventricular walls. *Clin. Anat.* **22**, 64-76.
Arteaga, G. M., Palmiter, K. A., Leiden, J. M. and Solaro, R. J. (2000). Attenuation of length dependence of calcium activation in myofilaments of transgenic mouse hearts expressing slow skeletal troponin I. *J. Physiol.* **526**, 541-549.
Azizi, E., Brainerd, E. L. and Roberts, T. J. (2008). Variable gearing in pennate muscles. *Proc. Natl. Acad. Sci. USA* **105**, 1745-1750.
Babu, A., Sonnenblick, E. and Gulati, J. (1988). Molecular basis for the influence of muscle length on myocardial performance. *Science* **240**, 74-76.
Bartol, I. K. (2001). Role of aerobic and anaerobic circular mantle muscle fibers in swimming squid: electromyography. *Biol. Bull.* **200**, 59-66.
Bartol, I. K., Krueger, P. S., Thompson, J. T. and Stewart, W. J. (2008). Swimming dynamics and propulsive efficiency of squids throughout ontogeny. *Integr. Comp. Biol.* **48**, 720-733.
Bartol, I. K., Krueger, P. S., Stewart, W. J. and Thompson, J. T. (2009). Hydrodynamics of pulsed jetting in juvenile and adult brief squid *Lolliguncula brevis*: evidence of multiple jet 'modes' and their implications for propulsive efficiency. *J. Exp. Biol.* **212**, 1889-1903.
Bone, Q. and Ryan, K. P. (1974). On the structure and innervation of the muscle bands of *Doliolum* (Tunicata: Cyclomyaria). *Proc. R. Soc. B* **187**, 315-327.
Bone, Q., Pulsford, A. and Chubb, A. D. (1981). Squid mantle muscle. *J. Mar. Biol. Assoc. U. K.* **61**, 327-342.
Bouligard, Y. (1966). La disposition des myofilaments chez une annélide polychète. *J. Microsc. (Paris)* **5**, 305-322.
Bower, J. R., Sakurai, Y., Yamamoto, J. and Ishii, H. (1999). Transport of the ommastrephid squid *Todarodes pacificus* under cold-water anesthesia. *Aquaculture* **170**, 127-130.
Brown, I. E., Cheng, E. J. and Loeb, G. E. (1999). Measured and modeled properties of mammalian skeletal muscle. II. The effects of stimulus frequency on force-length and force-velocity relationships. *J. Muscle Res. Cell Motil.* **20**, 627-643.
Burkholder, T. J. and Lieber, R. L. (2001). Sarcomere length operating range of vertebrate muscles during movement. *J. Exp. Biol.* **204**, 1529-1536.
Candia Carnevali, M. D., Saita, A. and Fedrigo, A. (1986). An unusual Z-system in the obliquely striated muscles of crinoids: three-dimensional structure and computer simulations. *J. Muscle Res. Cell Motil.* **7**, 568-578.
Cerri, P. S. and Sasso-Cerri, E. (2003). Staining methods applied to glycol methacrylate embedded tissue sections. *Micron* **34**, 365-372.
Chapple, W. D. (1983). Mechanical responses of a crustacean slow muscle. *J. Exp. Biol.* **107**, 367-383.
Clark, R. B. 1964. *Dynamics in Metazoan Evolution*. Oxford: Clarendon Press.
DeEguileor, M. and Valvassori, R. (1977). Studies on the helical and paramyosinic muscles. VII. Fine structure of body wall muscles in Sipunculus nudus. *J. Submicrosc. Cytol.* **9**, 363-372.
Eakin, R. M. and Brandenburger, J. L. (1974). Ultrastructural features of a gordian worm (Nematomorpha). *J. Ultrastruct. Res.* **46**, 351-374.
Fromherz, S. and Szent-Györgyi, A. G. (1995). Role of essential light chain EF hand domains in calcium binding and regulation of scallop myosin. *Proc. Natl. Acad. Sci. USA* **92**, 7652-7656.
Fukuda, N., Sasaki, D., Ishiwata, S. and Kurihara, S. (2001). Length dependence of tension generation in rat skinned cardiac muscle: role of titin in the Frank-Starling mechanism of the heart. *Circulation* **104**, 1639-1645.
Fukuda, N., Wu, Y., Farman, G., Irving, T. C. and Granzier, H. (2003). Titin isoform variance and length dependence of activation in skinned bovine cardiac muscle. *J. Physiol.* **553**, 147-154.
Gerry, S. P. and Ellerby, D. J. (2011). Serotonin modulates muscle function in the medicinal leech *Hirudo verbana*. *Biol. Lett.* **7**, 885-888.
Gordon, A. M., Homsher, E. and Regnier, M. (2000). Regulation of contraction in striated muscle. *Physiol. Rev.* **80**, 853-924.
Gosline, J. M. and Shadwick, R. E. (1983). The role of elastic energy storage mechanisms in swimming: an analysis of mantle elasticity in escape jetting in the squid, *Loligo opalescens*. *Can. J. Zool.* **61**, 1421-1431.
Gosline, J. M., Steeves, J. D., Harman, A. D. and DeMont, M. E. (1983). Patterns of circular and radial mantle muscle activity in respiration and jetting of the squid *Loligo opalescens*. *J. Exp. Biol.* **104**, 97-109.
Granzier, H. L., Akster, H. A. and Ter Keurs, H. E. (1991). Effect of thin filament length on the force-sarcomere length relation of skeletal muscle. *Am. J. Physiol.* **260**, C1060-C1070.
Hanft, L. M. and McDonald, K. S. (2010). Length dependence of force generation exhibit similarities between rat cardiac myocytes and skeletal muscle fibres. *J. Physiol.* **588**, 2891-2903.
Hidaka, T., Kuriyama, H. and Yamamoto, T. (1969). The mechanical properties of the longitudinal muscle in the earthworm. *J. Exp. Biol.* **50**, 431-443.
Houdusse, A., Kalabokis, V. N., Himmel, D., Szent-Györgyi, A. G. and Cohen, C. (1999). Atomic structure of scallop myosin subfragment S1 complexed with MgADP: a novel conformation of the myosin head. *Cell* **97**, 459-470.
Jahromi, S. S. and Atwood, H. L. (1969). Correlation of structure, speed of contraction, and total tension in fast and slow abdominal muscle fibers of the lobster (*Homarus americanus*). *J. Exp. Zool.* **171**, 25-37.
Josephson, R. K. (1975). Extensive and intensive factors determining the performance of striated muscle. *J. Exp. Zool.* **194**, 135-153.
Kier, W. M. (1982). The functional morphology of the musculature of squid (Loliginidae) arms and tentacles. *J. Morphol.* **172**, 179-192.
Kier, W. M. (1985). The musculature of squid arms and tentacles: ultrastructural evidence for functional differences. *J. Morphol.* **185**, 223-239.
Kier, W. M. and Curtin, N. A. (2002). Fast muscle in squid (*Loligo pealei*): contractile properties of a specialized muscle fibre type. *J. Exp. Biol.* **205**, 1907-1916.
Kier, W. M. and Schachat, F. H. (1992). Biochemical comparison of fast- and slow-contracting squid muscle. *J. Exp. Biol.* **168**, 41-56.
Kier, W. M. and Schachat, F. H. (2008). Muscle specialization in the squid motor system. *J. Exp. Biol.* **211**, 164-169.
Kuga, H. and Matsuno, A. (1988). Ultrastructural investigations on the anterior adductor muscle of a brachiopoda, *Lingula unguis*. *Cell Struct. Funct.* **13**, 271-279.
Lanzavecchia, G. (1977). Morphological modulations in helical muscles (Aschelminthes and Annelida). *Int. Rev. Cytol.* **51**, 133-186.
Lanzavecchia, G. and Arcidiacono, G. (1981). Contraction mechanism of helical muscles: experimental and theoretical analysis. *J. Submicrosc. Cytol.* **13**, 253-266.
Lanzavecchia, G. and De Eguileor, M. (1976). Studies on the helical and paramyosinic muscles. Part V. *J. Submicrosc. Cytol.* **8**, 69-88.
Lanzavecchia, G., Valvassori, R., de Eguileor, M. and Lanzavecchia, P., Jr (1979). Three-dimensional reconstruction of the contractile system of the Nematomorpha muscle fiber. *J. Ultrastruct. Res.* **66**, 201-223.
Layland, J., Young, I. S. and Altringham, J. D. (1995). The length dependence of work production in rat papillary muscles *in vitro*. *J. Exp. Biol.* **198**, 2491-2499.
Lunkenheimer, P. P., Redmann, K., Florek, J., Fassnacht, U., Cryer, C. W., Wübbeling, F., Niederer, P. and Anderson, R. H. (2004). The forces generated within the musculature of the left ventricular wall. *Heart* **90**, 200-207.
MacRae, E. K. (1965). The fine structure of muscle in a marine turbellarian. *Z. Zellforsch.* **68**, 348-362.
Malamud, J. G. (1989). The tension in a locust flight muscle at varied muscle lengths. *J. Exp. Biol.* **144**, 479-494.
Marsh, R. L. and Olson, J. M. (1994). Power output of scallop adductor muscle during contractions replicating the in vivo mechanical cycle. *J. Exp. Biol.* **193**, 139-156.
Matsuno, A. and Kuga, H. (1989). Ultrastructure of muscle cells in the adductor of the boring clam *Tridacna crocea*. *J. Morphol.* **200**, 247-253.
McDonald, K. S. and Moss, R. L. (1995). Osmotic compression of single cardiac myocytes eliminates the reduction in Ca^{2+} sensitivity of tension at short sarcomere length. *Circ. Res.* **77**, 199-205.

McDonald, K. S., Field, L. J., Parmacek, M. S., Soonpaa, M., Leiden, J. M. and Moss, R. L. (1995). Length dependence of Ca^{2+} sensitivity of tension in mouse cardiac myocytes expressing skeletal troponin C. *J. Physiol.* **483**, 131-139.
Miller, J. B. (1975). The length-tension relationship of the dorsal longitudinal muscle of a leech. *J. Exp. Biol.* **62**, 43-53.
Milligan, B., Curtin, N. and Bone, Q. (1997). Contractile properties of obliquely striated muscle from the mantle of squid (Alloteuthis subulata) and cuttlefish (*Sepia officinalis*). *J. Exp. Biol.* **200**, 2425-2436.
Mommsen, T. P., Ballantyne, J., Macdonald, D., Gosline, J. and Hochachka, P. W. (1981). Analogues of red and white muscle in squid mantle. *Proc. Natl. Acad. Sci. USA* **78**, 3274-3278.
Moon, T. W. and Hulbert, W. C. (1975). The ultrastructure of the mantle musculature of the squid *Symplectoteuthis oualaniensis*. *Comp. Biochem. Physiol.* **52B**, 145-149.
Norenburg, J. L. and Roe, P. (1998). Observations on musculature in pelagic nemerteans and on pseudostriated muscle in nemerteans. *Hydrobiologia* **356**, 109-120.
O'Dor, R. K. and Shadwick, R. E. (1989). Squid, the olympian cephalopods. *J. Cephalopod Biol.* **1**, 33-55.
Olson, J. M. and Marsh, R. L. (1993). Contractile properties of the striated adductor muscle in the bay scallop *Argopecten irradians* at several temperatures. *J. Exp. Biol.* **176**, 175-193.
Paps, J., Baguñà, J. and Riutort, M. (2009). Lophotrochozoa internal phylogeny: new insights from an up-to-date analysis of nuclear ribosomal genes. *Proc. Biol. Sci.* **276**, 1245-1254.
Preuss, T., Lebaric, Z. N. and Gilly, W. F. (1997). Post-hatching development of circular mantle muscles in the squid *Loligo opalescens*. *Biol. Bull.* **192**, 375-387.
Rack, P. M. H. and Westbury, D. R. (1969). The effects of length and stimulus rate on tension in the isometric cat soleus muscle. *J. Physiol.* **204**, 443-460.
Rieger, R. M. and Mainitz, M. (1977). Comparative fine structure study of the body wall in Gnathostomulida and their phylogenetic position between Platyhelminthes and Aschelminthes. *J. Zoolog. Syst. Evol. Res.* **15**, 9-35.
Rieger, R. M., Ruppert, E., Rieger, G. E. and Schoepfer-Sterrer, C. (1974). On the fine structure of gastrotrichs with description of *Chordodasys antennatus* sp.n. *Zool. Scr.* **3**, 219-237.
Rome, L. C. and Sosnicki, A. A. (1991). Myofilament overlap in swimming carp. II. Sarcomere length changes during swimming. *Am. J. Physiol.* **260**, C289-C296.
Rosenbluth, J. (1965). Ultrastructural organization of obliquely striated muscle fibers in *Ascaris lumbricoides*. *J. Cell Biol.* **25**, 495-515.
Rosenbluth, J. (1968). Obliquely striated muscle. IV. Sarcoplasmic reticulum, contractile apparatus, and endomysium of the body muscle of a polychaete, *Glycera*, in relation to its speed. *J. Cell Biol.* **36**, 245-259.
Rosenbluth, J. (1972). Obliquely striated muscle. In *The Structure and Function of Muscle,* Vol. 1, 2nd edn (ed. G. H. Bourne), pp. 389-420. New York, NY: Academic Press.
Rosenbluth, J., Szent-Györgyi, A. G. and Thompson, J. T. (2010). The ultrastructure and contractile properties of a fast-acting, obliquely striated, myosin-regulated muscle: the funnel retractor of squids. *J. Exp. Biol.* **213**, 2430-2443.
Roszek, B., Baan, G. C. and Huijing, P. A. (1994). Decreasing stimulation frequency-dependent length-force characteristics of rat muscle. *J. Appl. Physiol.* **77**, 2115-2124.
Rubenson, J., Pires, N. J., Loi, H. O., Pinniger, G. J. and Shannon, D. G. (2012). On the ascent: the soleus operating length is conserved to the ascending limb of the force-length curve across gait mechanics in humans. *J. Exp. Biol.* **215**, 3539-3551.
Shadwick, R. E. and Syme, D. A. (2008). Thunniform swimming: muscle dynamics and mechanical power production of aerobic fibres in yellowfin tuna (*Thunnus albacares*). *J. Exp. Biol.* **211**, 1603-1611.
Shaffer, J. F. and Kier, W. M. (2012). Muscular tissues of the squid *Doryteuthis pealeii* express identical myosin heavy chain isoforms: an alternative mechanism for tuning contractile speed. *J. Exp. Biol.* **215**, 239-246.
Szent-Györgyi, A. G. (2007). Regulation by myosin: how calcium regulates some myosins, past and present. In *Regulatory Mechanisms of Striated Muscle Contraction* (ed. S. Ebashi and I. Ohtsuki), pp. 253-264. New York, NY: Springer.
Tashiro, N. and Yamamoto, T. (1971). The phasic and tonic contraction in the longitudinal muscle of the earthworm. *J. Exp. Biol.* **55**, 111-122.
Terui, T., Sodnomtseren, M., Matsuba, D., Udaka, J., Ishiwata, S., Ohtsuki, I., Kurihara, S. and Fukuda, N. (2008). Troponin and titin coordinately regulate length-dependent activation in skinned porcine ventricular muscle. *J. Gen. Physiol.* **131**, 275-283.
Teuchert, G. (1974). Light and electron microscopical features of the muscular system from *Turbanella cornuta* (Gastrotricha, Macrodaysoidea). *Mikrofauna des Meeresbodens* **39**, 1-26.
Thompson, J. T. and Kier, W. M. (2006). Ontogeny of mantle musculature and implications for jet locomotion in oval squid *Sepioteuthis lessoniana*. *J. Exp. Biol.* **209**, 433-443.
Thompson, J. T., Szczepanski, J. A. and Brody, J. (2008). Mechanical specialization of the obliquely striated circular mantle muscle fibres of the long-finned squid *Doryteuthis pealeii*. *J. Exp. Biol.* **211**, 1463-1474.
Thompson, J. T., Taylor, K. R. and Gentile, C. (2010a). Gradients of strain and strain rate in the hollow muscular organs of soft-bodied animals. *Biol. Lett.* **6**, 482-485.
Thompson, J. T., Bartol, I. K., Baksi, A. E., Li, K. Y. and Krueger, P. S. (2010b). The ontogeny of muscle structure and locomotory function in the long-finned squid *Doryteuthis pealeii*. *J. Exp. Biol.* **213**, 1079-1091.
Toida, N., Kuriyama, H., Tashiro, N. and Ito, Y. (1975). Obliquely striated muscle. *Physiol. Rev.* **55**, 700-756.
Tu, M. S. and Daniel, T. L. (2004). Cardiac-like behavior of an insect flight muscle. *J. Exp. Biol.* **207**, 2455-2464.
van Leeuwen, J. L., van der Meulen, T., Schipper, H. and Kranenbarg, S. (2008). A functional analysis of myotomal muscle-fibre reorientation in developing zebrafish *Danio rerio*. *J. Exp. Biol.* **211**, 1289-1304.
Wainwright, S. A. (1988). *Axis and Circumference. The Cylindrical Shape of Plants and Animals*. Cambridge, MA: Harvard University Press.
Wakeling, J. M. and Johnston, I. A. (1999). White muscle strain in the common carp and red to white muscle gearing ratios in fish. *J. Exp. Biol.* **202**, 521-528.
Ward, D. V. (1972). Locomotory function of the squid mantle. *J. Zool.* **167**, 487-499.
Ward, D. V. and Wainwright, S. A. (1972). Locomotory aspects of squid mantle structure. *J. Zool.* **167**, 437-449.
Ward, S. M., McKerr, G. and Allen, J. M. (1986). Structure and ultrastructure of muscle systems within *Grillotia erinaceus* metacestodes (Cestoda: Trypanorhyncha). *Parasitology* **93**, 587-597.
Williams, C. D., Salcedo, M. K., Irving, T. C., Regnier, M. and Daniel, T. L. (2013). The length-tension curve in muscle depends on lattice spacing. *Proc. Biol. Sci.* **280**, 20130697.
Winegrad, S. (1974). Resting sarcomere length-tension relation in living frog heart. *J. Gen. Physiol.* **64**, 343-355.
Xie, X., Harrison, D. H., Schlichting, I., Sweet, R. M., Kalabokis, V. N., Szent-Györgyi, A. G. and Cohen, C. (1994). Structure of the regulatory domain of scallop myosin at 2.8 A resolution. *Nature* **368**, 306-312.

The Journal of Experimental Biology

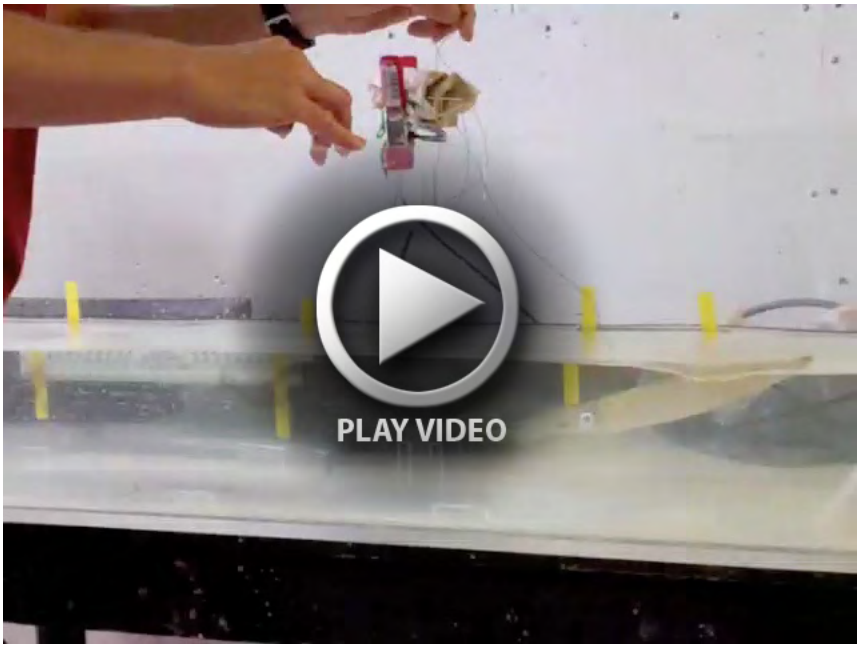

Movie 1. Escape jet. Two escape jets performed by an adult *Doryteuthis pealeii*. The sonomicrometry transducer leads are visible in the experimenter's hand.

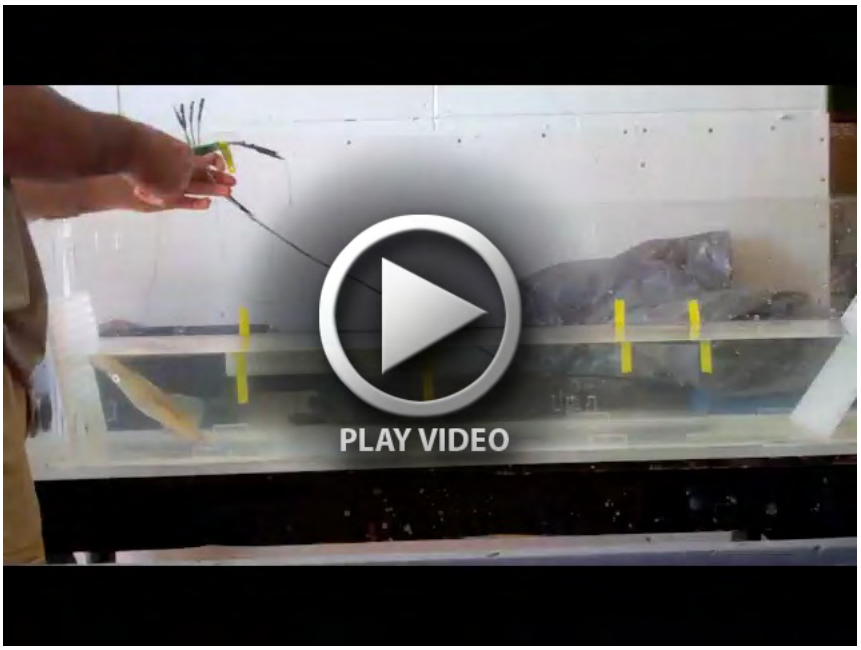

Movie 2. Slow swimming. Slow (i.e. less than 1.0 dorsal mantle lengths per second) rearward and forward swimming by an adult *Doryteuthis pealeii*. The sonomicrometry transducer leads are visible in the experimenter's hand.